Simulation of dielectric barrier discharge actuator at low Reynolds number

Nima Vaziri
Department of Physics, Karaj Branch, Islamic Azad University, Karaj, Iran
Ming-Jyh Chern
Department of Mechanical Engineering, National Taiwan University of Science and Technology, Taipei, Taiwan
Tzyy-Leng Horng
Department of Applied Mathematics, Feng Chia University, Taichung, Taiwan, and
Syamsuri Syamsuri
Department of Mechanical Engineering, Institut Teknologi Adhi Tama, Surabaya, Indonesia

Abstract

Purpose – The purpose of this study is to the modeling of the dielectric barrier discharge (DBD) actuator on the Eppler 387 (E387) airfoil in low Reynolds number conditions.

Design/methodology/approach – A validated direct-forcing immersed boundary method is used to solve the governing equations. A linear electric field model is used to simulate the DBD actuator. A ray-casting technique is used to define the geometry.

Findings – The purposed model is validated against the former studies. Next, the drag and lift coefficients in the static stall of the E387 airfoil are investigated. Results show that when the DBD actuator is on, both of the coefficients are increased. The effects of the location, applied voltage and applied frequency are also studied and find that the leading-edge actuator with higher voltage and frequency has better improvement in the forces. Finally, the dynamic stall of the E387 with the DBD actuator is considered. The simulation shows that generally when the DBD is on, the lift coefficient in the pitch-up section has lower values and in the pitch-down has higher values than the DBD off mode.

Practical implications – It is demonstrated that using the DBD actuator on E387 in the low Reynolds number condition can increase the lift and drag forces. Therefore, the application of the airfoil must be considered.

Originality/value – The results show that sometimes the DBD actuator has different effects on E387 airfoil in low Reynolds number mode than the general understanding of this tool.

Keywords Dynamic stall, Direct-forcing immersed boundary method, Dielectric barrier discharge actuator

Paper type Research paper

Introduction

There are many control technologies of the flow to improve the performances of the fluid machinery. Dielectric barrier discharge (DBD) plasma actuator is one of the effective devices to control the separation flow. The plasma actuator consists of two thin parallel-plate electrodes that are spaced by a dielectric material. A configuration of the DBD plasma actuator is shown in Figure 1. The electrodes are supplied with a high voltage. Therefore, the air in the region of the covered electrode is weakly ionized and the plasma is created. The plasma in the presence of an electric field has a large mean kinetic energy. It can produce a body force that causes a change in the velocity and the pressure distribution in this region. DBD actuators are easily installed. They also can transform into different shapes. Moreover, plasma actuators have not moved parts and they are stable in the atmospheric pressure because of the self-limiting.

The study of DBD plasma actuators has been started with the experiments of Corke *et al.* (2002) and Roth *et al.* (1998, 2000). As then, many researchers have been interested in this area. A plenty of experimental studies (Post and Corke, 2004; Corke and Post, 2005; Lombardi *et al.*, 2013; Mitsuo *et al.*, 2013; Fukumoto *et al.*, 2016) have been done in different applications of the DBD actuator such as the lift increasing on the wings, separation control on the turbine blades and control of the dynamic stall on the airfoils. Also, there are some DBD body force models (Massines *et al.*, 1998; Shyy *et al.*, 2002; Suzen *et al.*, 2005; Orlov, 2006; Phan and Shin, 2016; Wang and Tsao, 2018). Corke *et al.* (2010) reviewed the physics and applications of the plasma actuators up to the publish date.

The increasing performance of the low Reynolds number aerodynamics is important in some applications such as the small air travelers. When the Reynolds number is less than 10^5, the flow conditions such as the flow separation can affect the

The current issue and full text archive of this journal is available on Emerald Insight at: **https://www.emerald.com/insight/1748-8842.htm**

Aircraft Engineering and Aerospace Technology
 [ISSN 1748-8842]
[DOI 10.1108/AEAT-09-2019-0184]

Received 9 September 2019
Revised 15 December 2019
Accepted 10 February 2020

Figure 1 Schematic of the DBD plasma actuator

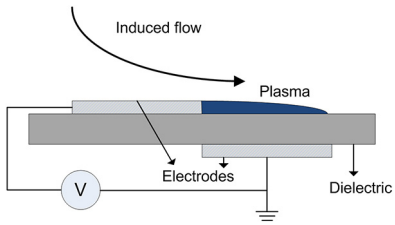

main aerodynamics parameters significantly. The DBD plasma actuator can be used to control the flow around the airfoil in this condition (Cho *et al.*, 2010; Cho and Shyy, 2011).

In our previous work, a direct-forcing immersed boundary (DFIB) method (Mohd-Yusof, 1996; Chern *et al.*, 2015) is used to simulate the static and the dynamic stall behaviors around the Eppler 387 (E387) airfoil in the low Reynolds number flow (Vaziri *et al.*, 2018). Low Reynolds number aerodynamics and airfoils (like the E387) is important in some applications such as the small airplanes, sailplanes, wind turbines and propellers. In the present study, the steady DBD plasma actuator is used for the model. The body force formulations are based on the Shyy *et al.* (2002) study. First, the new development is validated with a simple flat plate and NACA 0015 numerical and experimental results. Next, the flow behavior with the plasma actuator in the static and dynamic stalls conditions of the E387 airfoil is studied. Most of the parameters are same as our former study for better comparison. Finally, the effects of the main parameters are investigated and discussed. The aim of the present work is the study of the DBD plasma actuator on one of the famous airfoils in the low Reynolds number condition. Also, the capability of the DFIB method in the complex fluid–solid interactions are investigated.

Mathematical model and numerical method

Incompressible Newtonian fluid flow is assumed. In DFIB model the momentum equation can be defined as:

$$\frac{\partial \mathbf{u}}{\partial t} + \nabla \cdot (\mathbf{uu}) = -\nabla p + \frac{1}{Re}\nabla^2 \mathbf{u} + \eta \mathbf{f} \tag{1}$$

where $\mathbf{u}$ and p are non-dimensional velocity and pressure, respectively. $\eta \mathbf{f}$ is the virtual force that exerted to the solids body. η shows the volume of solid function. Inside the solid cell $\eta = 1$ and while the cell is fully occupied by fluids, η will be 0. The computational domain is two-dimensional and a ray-casting algorithm (Sutherland *et al.*, 1974) is used to define the solid cells (airfoil in the present study). The body forcing term $\mathbf{f}$ is specified by the difference between the interpolated velocity on the boundary point and the desired boundary velocity. A staggered grid arrangement is used in this study. The Adam–Bashforth, the second-order central difference and the third-order quadratic upstream interpolation for convective kinetics schemes are used for the temporal, the diffusive and the convective terms, respectively. The integration of the virtual force is used to calculate the resultant force applied to the solid object. Also, the drag and lift coefficients are two times of the resultant force in x and y-directions, respectively. More details in the DFIB model can be found in Chern *et al.* (2014, 2015). Furthermore, details of the ray-casting algorithm are given by Vaziri *et al.* (2018).

Dielectric barrier discharge actuator model

As mentioned previously, the DBD actuator model is based on the Shyy *et al.* (2002) formulation. In this model, the electric field is linear and the net charge density is constant. Figure 2 shows a simple DBD model on the E387 airfoil. The localized body force because of the plasma region is created in the triangle area.

The electric field can be calculated with:

$$\mathbf{E}'\left(x', y', t\right) = \left(\frac{|\mathbf{E}'(x', y', t)|k_2}{\sqrt{k_1^2 + k_2^2}}, \frac{|\mathbf{E}'(x', y', t)|k_1}{\sqrt{k_1^2 + k_2^2}}, 0\right) \tag{2}$$

where:

$$\mathbf{E}'\left(x', y', t\right) = E_0(t) - k_1 x' - k_2 y' \tag{3}$$

and

$$E_0(t) = \frac{V(t)}{d}. \tag{4}$$

In above equations x' and y' shows local coordinate system directions, k_1 and k_2 are the linearized slops of the electric field in x and y-directions, Also, E_0 is the maximum electric field, which is defined based on the applied voltage (V) and the insulator thickness (d). The electric field sets to zero outside the boundary of the plasma region. The body force because of the DBD actuator is defined as the:

$$\mathbf{F}_b(x, y, t) = \rho_c q_c \delta(x, y) f_v \Delta t_d \mathbf{E}(x, y, t) \tag{5}$$

Figure 2 DBD plasma actuator model on the airfoil

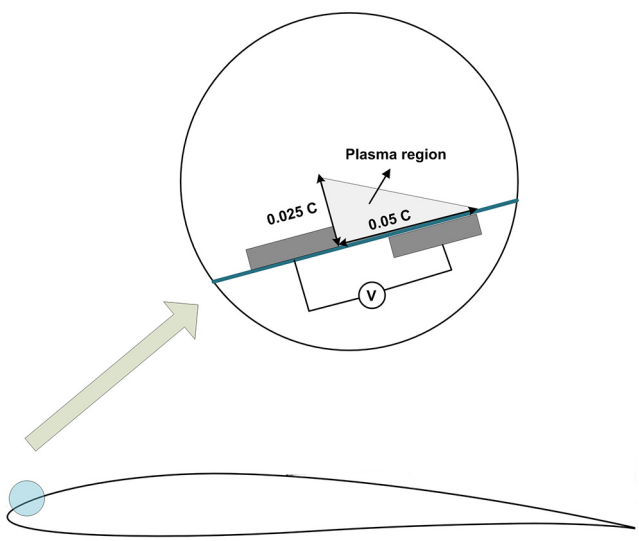

where ρ_c is the charge density, q_c is the unit charge, $\delta(x, y)$ is set to 1 inside the plasma region and 0 outside of that, f_v is the AC frequency of applied voltage, Δt_d is the discharge duty cycle and $\mathbf{E}(x, y, t)$ is the electric field distribution based on the equation (2). The non-dimensional form of the body force is added to the momentum equation (1).

In the present study, for the main cases, the horizontal length of the plasma field is set to the 0.05 of the chord and the vertical length is set to the 0.025 of the chord. Other main parameters required here are, the frequency of applied voltage is 3 kHz, the charge density is $1 \times 10^{15}/\text{cm}^3$, the applied voltage is 7 kV, the discharge duty cycle is 67 μs and the insulator thickness is set to the 0.025 of the chord. More details about the above model can be found in Shyy *et al.* (2002), Cho *et al.* (2010) and Cho and Shyy (2011).

Results and discussion

The basic model (without the DBD actuator force scheme) was validated in our former studies (Chern *et al.*, 2015; Vaziri *et al.*, 2018). In this section, the model is validated with the numerical and the experimental results. Next, the static and dynamic stalls of the E387 are considered. The effect of the DBD force and the main parameters of that are studied and discussed.

Validation

First, flow over a small flat plate is considered. The length of the plate (L) is 10 and this value is used as a non-dimensional length unit. The plasma region is created on the center of the upper side of the plate with a length of 0.3 L and a height of 0.15 L (Figure 3). The Dirichlet boundary condition is applied at the inlet boundary and Neumann boundary conditions are applied at lateral and outlet sides. The non-dimensional inlet velocity value is set to one. The main parameters of the plasma field are followed by the DBD actuator model section values. The Reynolds number and the applied voltage are 27.4 and 5.66 kV, respectively, and the final body force is non-dimensionalized and used in the momentum equation (Shyy *et al.*, 2002). The grid resolution is 1,000 × 500.

Figure 4 shows the comparison of the velocity profile at the end of the plasma region between the present study and Shyy *et al.* (2002). U is the flow velocity parallel to the wall and U_∞ is the inlet velocity. It can be seen that the present results are in agreement with the reduced-order DBD model of the Shyy. The present model almost over predicts the actuator effect. Figures 5 and 6 depict the contours of the non-dimensional form of the x-velocity component (U) and the pressure in the upper part of the flat plate. The plasma field is created inside the triangle. It can be seen that the body force is generated in the plasma region. Therefore, the pressure reduces inside the region. The decrease is linear due to the structure of

Figure 3 The computational domain of the flat plate case (the figure is not scaled)

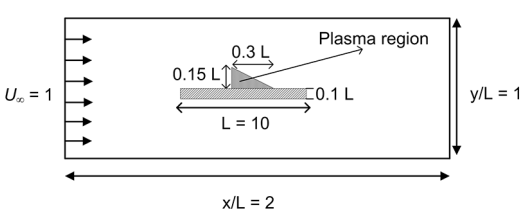

Note: The figure is not scaled

Figure 4 Comparison of the horizontal component of the velocity profile at the end of the actuator region

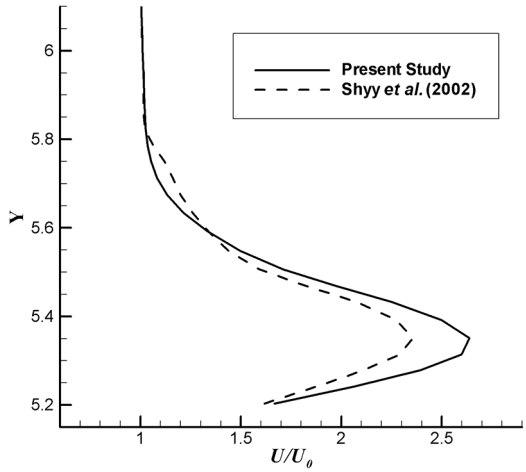

Figure 5 Non-dimensional velocity contour on the upper side of the flat plate

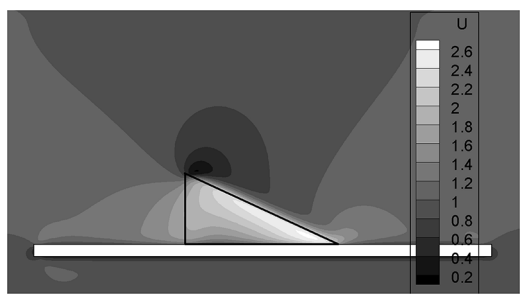

Note: The triangle shows the plasma region

Figure 6 Non-dimensional pressure contour on the upper side of the flat plate

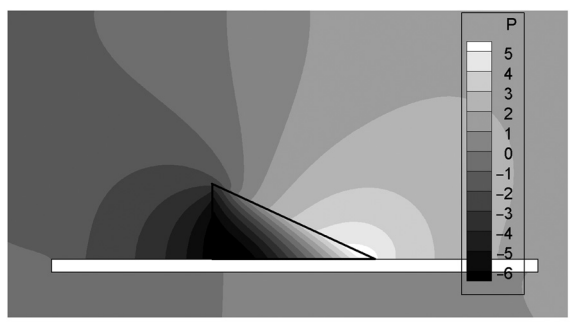

Note: The triangle shows the plasma region

the model. On the other hand, as it is expected, the value of the horizontal component of the velocity is increased.

Now, the model is used to NACA 0015 airfoil. The actuator is on the leading of the airfoil (Figure 2). The Reynolds number is set to 217,000 and the angle of attacks change from 0° to 12°. The comparison of the lift coefficients with former studies of Corke *et al.* (2004) and Voikov *et al.* (2004) can be seen in Figure 7. It should be noted that in the Corke results, the plasma actuator is off and in the Voikov study, the plasma actuator is on and steady. Generally, the present studies are in agreement with the former results. Also, the lift coefficient is increased when the plasma actuator is on and the extra body force is created. However, it should be noted that the laminar model is used in the present study and all of the results may be a change in turbulent conditions.

Static stall – Eppler 387

Now, the E387 airfoil is considered. The leading-edge steady actuator with the applied voltage of 7,000 V is used. The Reynolds number is set to 60,000. The angles of attacks are from −2 to 12. Other main parameters, such as a domain size (8*c to 4*c, that c is the chord size of the airfoil and set to one) and boundary conditions are same as the Vaziri *et al.* (2018) study. The DBD actuator settings are similar to the values in the DBD actuator model section. The aim of the study is investigation of the plasma field on the drag and lift coefficients of the E387 as a usual low Reynolds number airfoil. Figures 8 and 9 shows the effect of the DBD actuator on the drag and lift coefficients. The drag coefficient is increased in most of the angles when the DBD actuator is on. The increasing rate is significantly for $\alpha > 8°$. Most of the experimental studies show that the drag coefficient is decreased in turbulent flow. The main reason is the effect of the DBD actuator on turbulent drag (Orlov, 2006). On the other hand, some investigations show contrary results, increasing of the drag coefficient with DBD actuator (Cho *et al.*, 2010; Mazaheri *et al.*, 2016; Fukumoto *et al.*, 2016). It is reported that the main reason is the additional wall shear stress in the plasma region. Also, the angle of attacks is one of the important parameters. The present study shows

Figure 7 Comparison of the lift coefficient versus angle of attacks for NACA 0015 with the leading-edge actuator

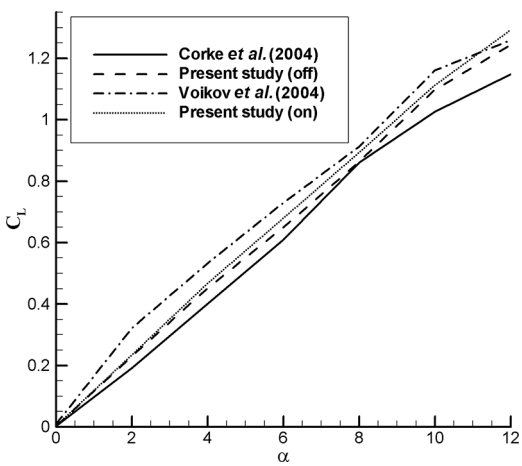

Figure 8 Comparison of the drag coefficient versus angle of attacks for E387 with the leading-edge actuator in Re = 60,000

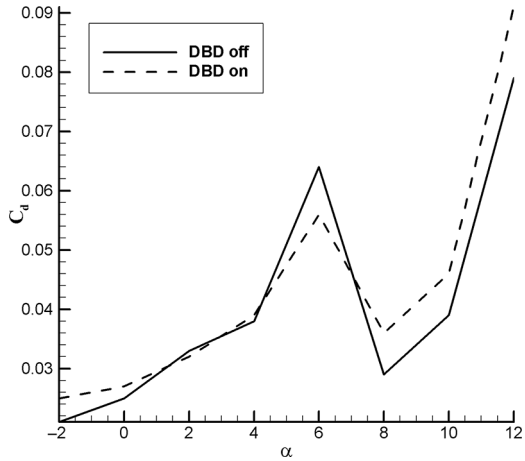

that the shape of the airfoil beside the other main parameters is very important in the low Reynolds number range. Therefore, the results of the DBD actuator on drag coefficient may be undesirable.

The effect of the plasma creation on the lift coefficient is depicted on Figure 9. As it is expected, the lift coefficient is increasing when the DBD actuator is on. The only exception (in this Reynolds number) is 4°. The main increasing rate is about 10 per cent.

Now, the effect of some important parameters of DBD actuator on the drag and lift coefficients are considered. The location of the electrodes is always questionable. Here, three main locations, the leading-edge, center of the airfoil and the trailing-edge are modeled. All of the parameters are the same as the previous case. Table I shows the effect of the location on C_d and C_l. The results represent in the point of view of the C_l/C_d, the trailing-edge actuator is more effective than the other cases; but on the other hand, the lift coefficient of the leading-edge actuator is better than the other cases. Former studies also

Figure 9 Comparison of the lift coefficient versus angle of attacks for E387 with the leading-edge actuator in Re = 60,000

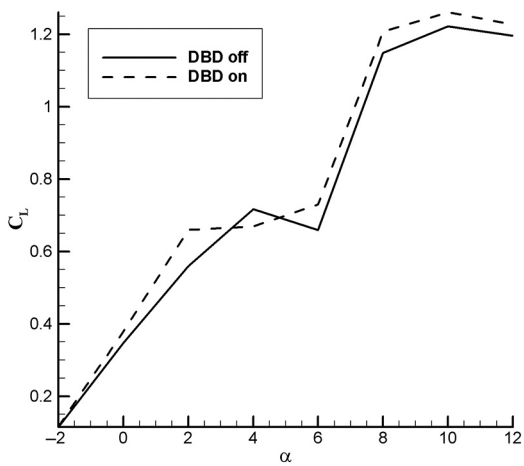

Table I The effect of the electrodes location on drag and lift coefficients

Location	C_d	C_l	C_l/C_d
Leading-edge	0.0620	1.2230	19.726
Center	0.0619	1.2224	19.748
Trailing-edge	0.0618	1.2227	19.785

show that generally, the leading-edge actuator is better than the others (Corke *et al.*, 2010).

Two other important parameters are the frequency of the applied voltage. Theoretically, the increase of the applied voltage increases the energy of the ionized gas in the plasma region, and therefore, the value of the flow velocity will be increased. Experiment evidence confirm this idea. In the present study, the applied voltage from 4 to 9 kV are used. Figure 10 shows the effect of applied voltage on the drag and lift coefficients. The results are in agreement with other reports (Shyy *et al.*, 2002; Corke *et al.*, 2010; Cho and Shyy, 2011). Studies about the AC frequency show that the optimized value of this quantity depends on the capacity of the actuator (Orlov *et al.*, 2006). The present results (Figure 11) demonstrate that the higher value of the frequency decreases the drag coefficient, and therefore, it will be more effective.

Dynamic stall – Eppler 387

In this section, the oscillation of E387 with DBD actuator is studied and the effects of main parameters are investigated. The pitching of the airfoil is based on the following equations (6) and (7):

$$\alpha = \alpha_{\text{mean}} + \alpha_{\text{amp}} \sin(2\pi f t), \tag{6}$$

and the reduced frequency is defined as:

$$k = \frac{\pi f c}{U_\infty}. \tag{7}$$

In above equations, α_{mean} is the mean angle of attack and set to 15, α_{amp} is the pitch oscillation amplitude and set to 30, f is the oscillation frequency, c is the chord size of the airfoil that is set to 1, k is equal to 2.0 and Re = 3,000. The main DBD parameters, the domain size and boundary condition are same as the main case of the previous section. Figure 12 depicts the effect of the DBD actuator on the lift coefficient in dynamic stall mode. The cycle of the case with the actuator off has been reported in our previous study (Vaziri *et al.*, 2018). In comparison with the actuator off-cycle, in the pitch-up section, the lift decreases with increasing of the angle of attacks up to approximately 40°. The sharp drop is occurred at $\alpha = 45$, as it is expected. In the pitch-down part, the lift coefficient is higher than the DBD off values at lower than the 40 angles of attacks. The former results in this area show various results. For example, Fukumoto *et al.* (2016, 2018) found almost the same trend as the present study in NACA 0012 with Re = 2.56×10^5. Mitsuo *et al.* (2013) experimental results also confirm the above outcomes. On the other hand, Corke and Post (2005) and Post and Corke (2004) obtained the higher lift coefficient in pitch-up and almost the lower one in pitch-down (in comparison with the DBD off in NACA 0015). Lombardi *et al.* (2013) also investigate the effect of different DBD actuator parameters on dynamic stall control. Based on the previous and the present studies, there is not any guaranty that the DBD actuator can improve the dynamic stall cycle. It highly depends on the Airfoil shape, the Reynolds number and the reduced frequency.

The effects of the DBD location, applied voltage and applied frequency on the dynamic stall control are also investigated. The other parameters are constant and the same as the main dynamic stall case. Figure 13 shows the lift coefficient versus the angle of attack in three main locations of the DBD actuator: the leading, the center and the trilling of the airfoil. The results represent that the trailing-edge actuator can control the dynamic stall better than the other locations, especially in the pitch-up section. Figures 14 and 15 depict the effects of the applied voltage and frequency. In contrary to the static stall cases, the consequences of changing these parameters are insignificant. Higher frequency and voltage can increase the lift in the pitch-up a little.

Conclusions

A validated DFIB method has been used to model the DBD actuator on the E387 airfoil in the low Reynolds number condition. The model was validated for the flat plate geometry against the former numerical study. Also, the static stall of the

Figure 10 Lift and drag coefficients in different values of the applied voltage at the angle of attack of 10

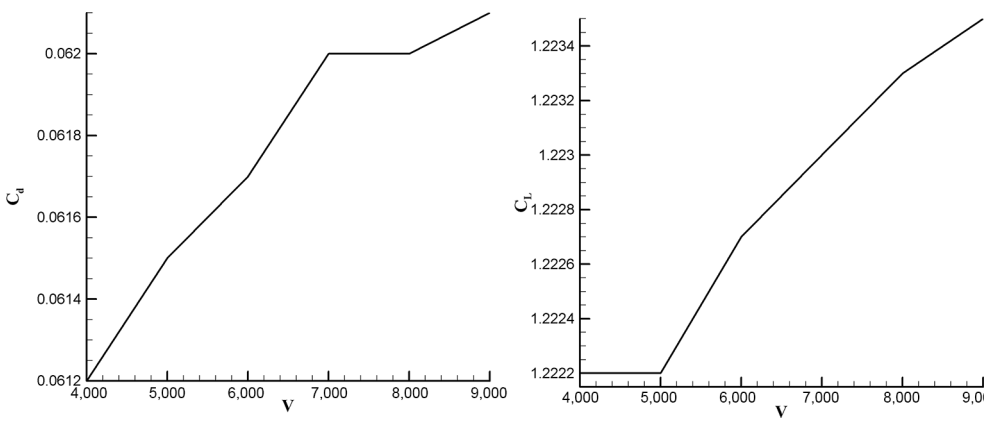

Figure 11 Lift and drag coefficients in different values of the AC frequency at the angle of attack of 10

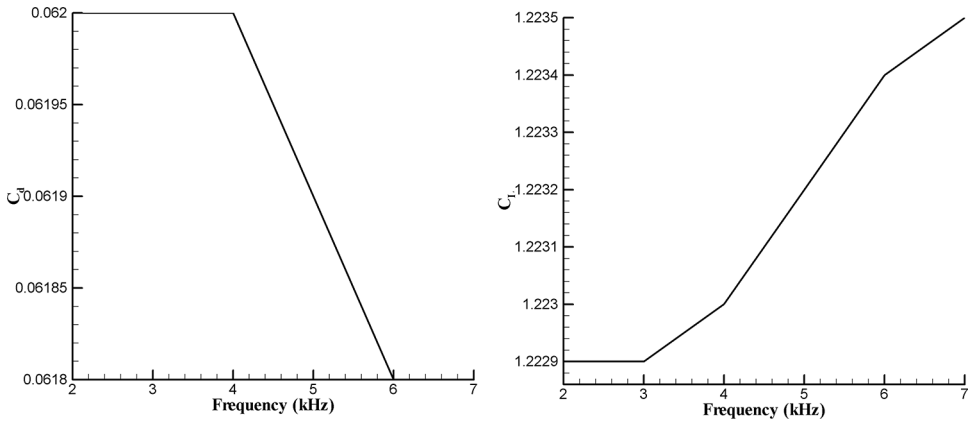

Figure 12 Comparison of the lift coefficient in the dynamic stall cycle with the plasma actuator off and on

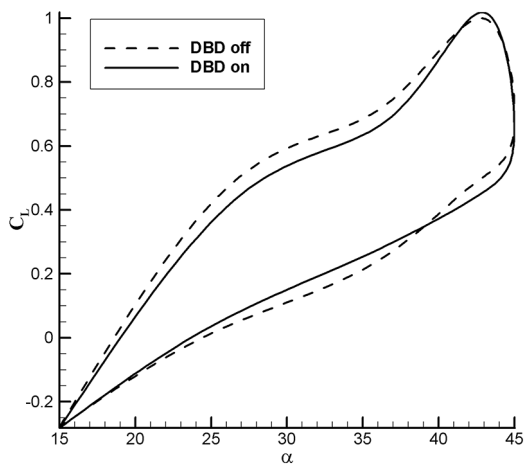

Figure 13 Comparison of the lift coefficient in the dynamic stall cycle with DBD on mode for different locations of the actuator

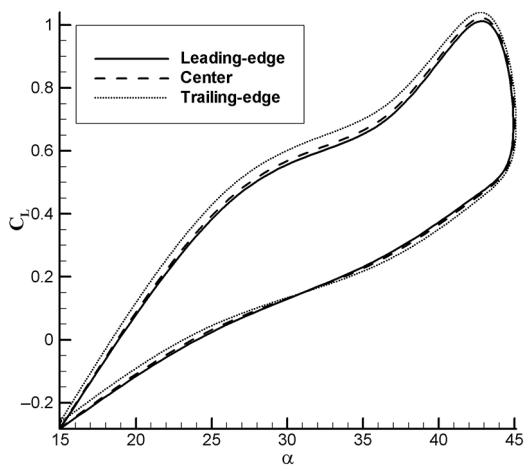

Figure 14 Comparison of the lift coefficient in the dynamic stall cycle with DBD on mode for different applied voltage

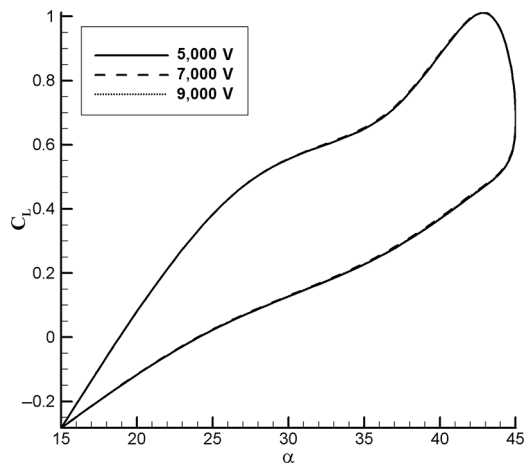

Figure 15 Comparison of the lift coefficient in the dynamic stall cycle with DBD on mode for different applied frequency

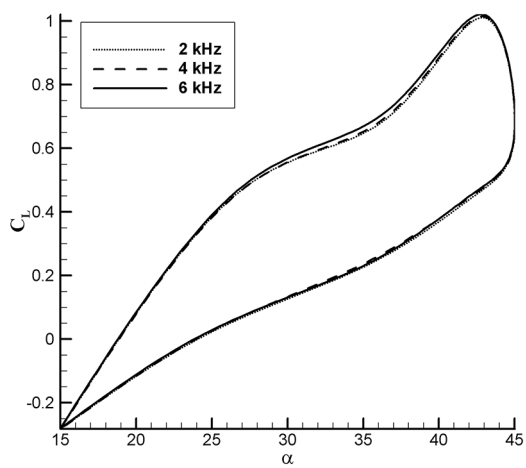

NACA 0015 was used for verification of the code in comparison with the experimental report. Next, the static stall of the E387 airfoil was considered. The Reynolds number was set to 6,000 and the drag and lift coefficients were calculated. Results showed that when the DBD actuator is on, both of the coefficients are increased. The study of the location of the DBD actuator represented that the increasing of the lift coefficient in the leading-edge condition is larger than the other locations; but in the point of view of Cl/Cd, the trilling-edge actuator has better improvement. Also, the study of the effect of the applied voltage and AC frequency showed that higher values of both parameters can enhance the force coefficients against the lower tested values. Finally, the dynamic stall of the E387 with the DBD actuator was considered. The Reynolds number and the reduced frequency were set to 3,000 and 2, respectively. The simulation showed that generally when the DBD is on, the Lift coefficient in the pitch-up section has lower values and in the pitch-down has higher values than the DBD off mode. Also, the best improvement occurs in the leading-edge location. The present study demonstrated that using the DBD actuator in the low Reynolds number condition generally can improve the lift force of the airfoil; but also, it can increase the drag force too. Therefore, the application of the airfoil must be considered. It should be noted that the present study just focuses on E387 airfoil.

References

Chern, M.J., Noor, D.Z., Liao, C.B. and Horng, T.L. (2015), "Direct-forcing immersed boundary method for mixed heat transfer", *Communications in Computational Physics*, Vol. 18 No. 4, pp. 1072-1094.

Chern, M.J., Kuan, Y.H., Nugroho, G., Lu, G.T. and Horng, T.L. (2014), "Direct-forcing immersed boundary modeling of vortex-induced vibration of a circular cylinder", *Journal of Wind Engineering and Industrial Aerodynamics*, Vol. 134, pp. 109-121.

Cho, Y.C. and Shyy, W. (2011), "Adaptive flow control of low-Reynolds number aerodynamics using dielectric barrier discharge actuator", *Progress in Aerospace Sciences*, Vol. 47 No. 7, pp. 495-521.

Cho, Y.C., Hoagg, J.B., Bernstein, D.S. and Shyy, W. (2010), "Retrospective cost adaptive control of low-Reynolds number aerodynamics using a dielectric barrier discharge actuator", *5th Flow Control Conference, Chicago, IL*.

Corke, T.C. and Post, M.L. (2005), "Overview of plasma flow control: concepts, optimization, and applications", *AIAA Aerospace Science Meeting Exhibition, 43th, Reno, NV*.

Corke, T.C., He, C. and Patel, M. (2004), "Plasma flaps and slats: an application of weakly-ionized plasma actuators", *AIAA Flow Control Conference, 2nd, Portland*.

Corke, T.C., Lon Enloe, C. and Wilkinson, S.P. (2010), "Dielectric barrier discharge plasma actuators for flow control", *Annual Review of Fluid Mechanics*, Vol. 42 No. 1, pp. 505-529.

Corke, T.C., Jumper, E.J., Post, M.L., Orlov, D. and McLaughlin, T.E. (2002), "Application of weakly-ionized plasmas as wing flow-control devices", *AIAA Aerospace Science Meeting Exhibition, 40th, Reno, NV*.

Fukumoto, H., Aono, H., Nonomura, T., Oyama, A. and Fujii, K. (2018), "Large-eddy simulations of flow control effects of a DBD plasma actuator at various burst frequencies on a dynamic flow field around a pitching NACA0012 airfoil at Reynolds number of 256,000", *AIAA Science Technology Forum, Kissimmee, FL*.

Fukumoto, H., Aono, H., Tanaka, M., Matsuda, H., Osako, T., Nonomura, T., Oyama, A. and Fujii, K. (2016), "Control of dynamically stalled flow eld around a pitching airfoil by DBD plasma actuator", *8th AIAA Flow Control Conference, Washington, DC*.

Lombardi, P., Bowles, O. and Corke, T.C. (2013), "Closed-Loop dynamic stall control using a plasma actuator", *AIAA Journal*, Vol. 51 No. 5.

Massines, F., Rabehi, A., Decomps, P., Gadri, R.B., Segur, P. and Mayoux, C. (1998), "Experimental and theoretical study of a glow discharge at atmospheric pressure controlled by dielectric barrier", *Journal of Applied Physics*, Vol. 83 No. 6, pp. 2950-2957.

Mazaheri, K., Omidi, J. and Kiani, K.C. (2016), "Simulation of DBD plasma actuator effect on aerodynamic performance improvement using a modified phenomenological model", *Computers & Fluids*, Vol. 140, pp. 371-384.

Mitsuo, K., Watanabe, S., Atobe, T. and Kato, H. (2013), "Lift enhancement of a pitching airfoil in dynamic stall by DBD plasma actuators", *51st AIAA Aerospace Sciences Meeting including the New Horizons Forum and Aerospace Exposition, Grapevine, TX*.

Mohd-Yusof, J. (1996), "Interaction of massive particles with turbulence", PhD. Dissertation, Dept. of Mechanical and Aerospace Engineering, Cornell University.

Orlov, D.M. (2006), "Modelling and simulation of single dielectric barrier discharge plasma actuators", PhD thesis, University of Notre Dame.

Orlov, D., Corke, T.C. and Patel, M. (2006), "Electric circuit model for aerodynamic plasma actuator", *AIAA Aerospace Science Meeting Exhibition, 44th, Reno, NV*.

Phan, M.K. and Shin, J. (2016), "Numerical investigation of aerodynamic flow actuation produced by surface plasma actuator on 2D oscillating airfoil", *Chinese Journal of Aeronautics*, Vol. 29 No. 4, pp. 882-892.

Post, M.L. and Corke, T.C. (2004), "Separation control on high angle of attack airfoil using plasma actuators", *AIAA Journal*, Vol. 42 No. 11, pp. 2177-2184.

Roth, J.R., Sherman, D. and Wilkinson, S. (1998), "Boundary layer flow control with one atmosphere uniform glow discharge surface plasma", *AIAA Aerospace Science Meeting Exhibition, 36th, Reno, NV*.

Roth, J.R., Sherman, D.M. and Wilkinson, S.P. (2000), "Electrohydrodynamic flow control with a glow-discharge surface plasma", *AIAA Journal*, Vol. 38 No. 7, pp. 1166-1172.

Shyy, W., Jayaraman, B. and Andersson, A. (2002), "Modeling of glow discharge-induced fluid dynamics", *Journal of Applied Physics*, Vol. 92 No. 11, pp. 6434-6443.

Sutherland, I., Sproull, R.F. and Schumacker, R.A. (1974), "A characterization of ten hidden-surface algorithms", *ACM Computing Surveys (CSUR)*, Vol. 6.

Suzen, Y.B., Huang, P.G., Jacob, J.D. and Ashpis, D.E. (2005), "Numerical simulations of plasma based flow

control applications", *AIAA Fluid Dynamic Conference Exhibition, 35th, Toronto*.

Vaziri, N., Chern, M.J. and Horng, T.L. (2018), "Simulation of dynamic stall using direct-forcing immersed boundary method at low Reynolds number", *Aircraft Engineering and Aerospace Technology*, Vol. 20.

Voikov, V., Corke, T.C. and Haddad, O. (2004), "Numerical simulation of flow control over airfoils using plasma actuators", *American Physics Society Division of Fluid Dynamics*, Vol. 49.

Wang, C.C. and Tsao, H.W. (2018), "Control of a turbulent non-premixed flame by plasma actuators", *Journal of Thermophysics and Heat Transfer*, Vol. 32 No. 1, pp. 111-117.

Corresponding author

Nima Vaziri can be contacted at: nima_vaziri@kiau.ac.ir